LTE-Based Channel Measurements for High-Speed Railway Scenarios

Tao Zhou[†], Cheng Tao[†§], Sana Salous[‡], Liu Liu[†], Zhenhui Tan[†]
[†]Institute of Broadband Wireless Mobile Communications, Beijing Jiaotong University, Beijing 100044, P.R.China
[‡]School of Engineering and Computing Sciences, Durham University, Durham, DH1 3LE, UK
[§]National Mobile Communications Research Laboratory, Southeast University, Nanjing 210096, P.R.China
Email: taozhou.china@gmail.com, chtao@bjtu.edu.cn, sana.salous@durham.ac.uk, {liuliu, zhhtan}@bjtu.edu.cn

***Abstract*—Channel measurements are the precondition for the design of future high-speed railway (HSR) communication systems. Due to the measurement restriction and measurement efficiency issues of applying conventional channel sounders in HSR scenarios, railway network based channel sounding methods are becoming quite attractive. In this paper, we employ long term evolution (LTE) railway network to achieve HSR channel measurements. A novel LTE-based HSR channel sounding system is proposed to enable the collection of time-frequency-space channel data. Field measurements that consider both direct and relay coverage schemes are conducted on Beijing to Tianjin HSR in China. Measurement data are partitioned into single-link case in which the common channel parameters can be derived and multi-link case in which the correlation between different links can be characterized. Measurement results cover path loss (PL), Ricean K-factor, delay spread, single-link and multi-link spatial correlation, which not only confirm the utility of the proposed system but also provide preliminary channel information available for the study of next generation HSR communication systems.**

I. Introduction

High speed railway (HSR) communication, divided into professional communication and public communication, is an important part in the whole HSR system. The professional communication aims to ensure the safety of railway operation, while public communication is in charge of passenger experience services such as Internet access, high-quality voice and mobile video broadcasting. The leading global system for mobile communications for railway (GSM-R) is primarily used for the train control data transmission, and it can only maintain low data rate communications. Professional broadband services, such as onboard video surveillance and track monitoring, as well as those regarding public services far exceed the capability of GSM-R. To meet these requirements, future HSR communication systems are envisioned to achieve professional and public broadband communications simultaneously [1][2].

Since the radio channel determines the performance of wireless communication systems, detailed knowledge and accurate characterization of its parameters in realistic HSR propagation scenarios is crucial. The majority of radio channel models used for system simulation are based on extensive channel measurement data. Therefore, channel measurements are the precondition for the design of HSR communication systems and the evaluation of HSR communication technologies.

Though measurement campaigns on HSR are expensive, time-consuming, and difficult to carry out, a few HSR channel measurements have been conducted, which can be classified into two categories, as follows:

1) Channel sounder based measurements. There are only several measurement campaigns taken under high mobility conditions, using standard commercial channel sounders, e. g., RUSK and Propsound. One of the first reported HSR measurements employed the RUSK sounder to measure the single-input multiple-output (SIMO) relay channel in Germany [3]. Propsound HSR channel measurements in rural and hilly scenarios in Taiwan were reported in [4]. The direct link was considered to measure the SIMO and the multiple-input single-output (MISO) channel. Further, single-input single-output (SISO) mobile relay channel measurements using Propsound were carried out in viaduct scenarios on HSR in China [5]. However, there are still no reported MIMO channel measurements in a specific HSR scenario utilizing standard commercial channel sounders.

2) Railway network based measurements. Due to some restrictions imposed by using traditional channel sounders on HSR [6], since 2011 some researchers resorted to the railway network based channel sounding method. A series of GSM-R channel measurements were conducted in viaduct scenarios on HSR in China [7]. For channel characterization purposes, the GSM-R signal is regarded as a narrowband continuous waveform (CW) signal and hence not suitable for wideband measurements. To enable the wideband channel characterization, the common pilot channel (CPICH) signal in the dedicated WCDMA network was collected and analyzed to extract the multipath properties [8]. Unfortunately, the measurement bandwidth of this method does not meet the requirements of future HSR communication systems [1], and it lacks the spatial sounding ability.

In fact, existing HSR channel measurement data are insufficient for the design of future HSR communication systems. It is necessary to carry out more measurements for the further HSR channel characterization. Reported measurement campaigns, do not provide a suitable approach with the potential of enabling comprehensive and efficient HSR channel measurements.

In recent years, there have been large-scale deployments of long term evolution (LTE) networks around the world. In particular, the LTE railway networks have almost covered all

978-1-4799-5952-5/15/$31.00 ©2015 IEEE

HSRs in China, for a total of 15,000 km by 2014, and as HSRs continue to grow, the LTE railway networks that grow with them will exceed 30,000 km in 2020 [9]. Based on the LTE railway networks, a novel HSR channel sounding scheme is first presented in [10] where the simulation results have confirmed the feasibility of the method.

The primary contribution of this paper is to implement LTE-based HSR measurements for characterizing HSR radio channels. A novel channel sounding system is proposed to enable the implementation of the LTE-based HSR channel sounding scheme. Based on the proposed system, field measurements are conducted to acquire channel data for propagation characterization. Finally, both large-scale and small-scale characteristics in two sorts of HSR coverage scenarios are analyzed and compared.

The remainder of this paper is outlined as follows. Section II introduces the LTE-based HSR channel sounding system. In Section III, LTE-based HSR measurement campaigns are described. According to the measurement data, HSR channel characterization is presented in Section IV. Finally, conclusions are drawn in Section V.

II. LTE-Based HSR Channel Sounding System

The proposed LTE-based HSR channel sounding system is shown in Fig. 1. This system consists of the LTE railway network and a LTE sounder. The LTE sounder is used to collect the channel data in the whole coverage area of the network, which makes continuous measurements feasible. Obvious advantages of this system are the high measurement efficiency and low measurement restriction.

Unlike the conventional cellular network, the railway network adopts a narrow strip coverage mode and a building baseband unit (BBU) plus remote radio unit (RRU) structure. One base station (BS) site has two RRUs which employ directional antennas to transmit radio frequency (RF) signals in opposite directions along the track. Cell combination technology [9] is used in this network, which combines several RRUs into a big narrow-strip-shaped cell via optical fiber. These RRUs are controlled by the BBU that is in charge of RF signal processing. Due to such dedicated structure, the whole network can be classified into two categories: non-overlapped coverage region and overlapped coverage region. In the non-overlapped coverage area, only one signal from one BS is received. In the overlapped area, however, the two same signals from neighboring BSs arrive at the receiver simultaneously. From the delay domain perspective, these signals can still be distinguished according to different propagation delays.

Cell-specific reference signal (CRS), as an essential component of the LTE signal, is used for channel estimation in the downlink. When it comes to channel sounding, the CRS can be regarded as a kind of excitation waveforms, whose signal structure determines the measurement capability. In [10], it has been evaluated that the CRS, with 18 MHz measurement bandwidth (56 ns time delay resolution), 11 us time delay window and 1 KHz maximum expected Doppler shift, is able to meet the requirements of HSR channel measurements.

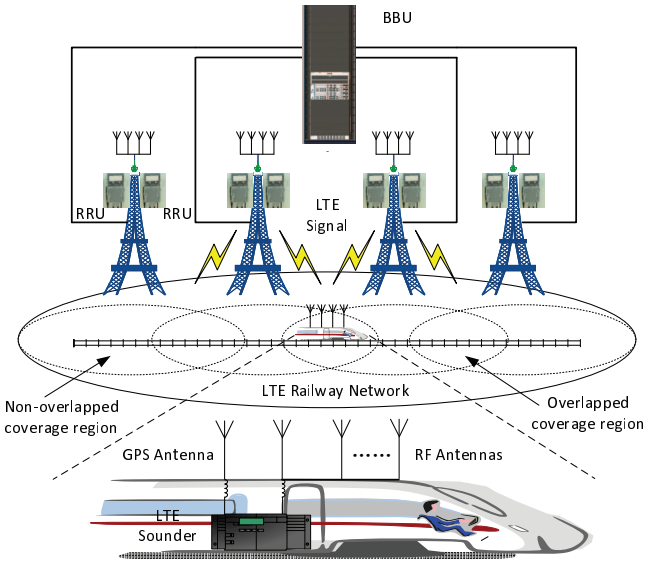

Fig. 1. LTE-based HSR channel sounding system.

Additionally, there exist 4 antenna ports carrying orthogonal CRSs, thus supporting the MIMO channel measurement.

Different from the conventional channel sounders, the LTE sounder has only receiver whose architecture is shown in Fig. 2. Full parallel architecture [11] that receives the excitation signal simultaneously from all antennas is employed. Basic functions, such as RF down conversion and data acquisition, are involved in the LTE sounder. In particular, GPS frequency reference is used to enable the frequency consistency between the LTE railway network and the LTE sounder. Also, LTE baseband data and navigation data are stored together in a solid state disk (SSD) for post processing. Frame and slot synchronization is implemented to acquire LTE frames and determine the cell identity (ID) for extracting the received CRS and generating the local CRS respectively. Since the CRS is OFDM modulated, frequency domain correlation [12] is used to estimate the CFR which can be subsequently transformed to the CIR by the inverse fast Fourier transform (IFFT) operation.

III. LTE-Based HSR Measurement Campaigns

Based on the proposed channel sounding system, the novel HSR channel measurements are conducted on Beijing to Tianjin (BT) HSR in China. In the following we describe the measurement campaigns in detail and then we partition the acquired measurement data into single-link and multi-link cases.

A. Measurement Description

The LTE network structure and propagation environment of BT HSR are illustrated in Fig. 3. The chosen network covers about 16 km distance with 15 BSs and 30 RRUs. The maximum spacing between BSs is around 1.2 km. There are two types of cell structures serving for 2605 MHz and 1890 MHz networks respectively. The 2605 MHz network has 6 cells, each of which contains 3 BSs or 2 BSs, whereas the

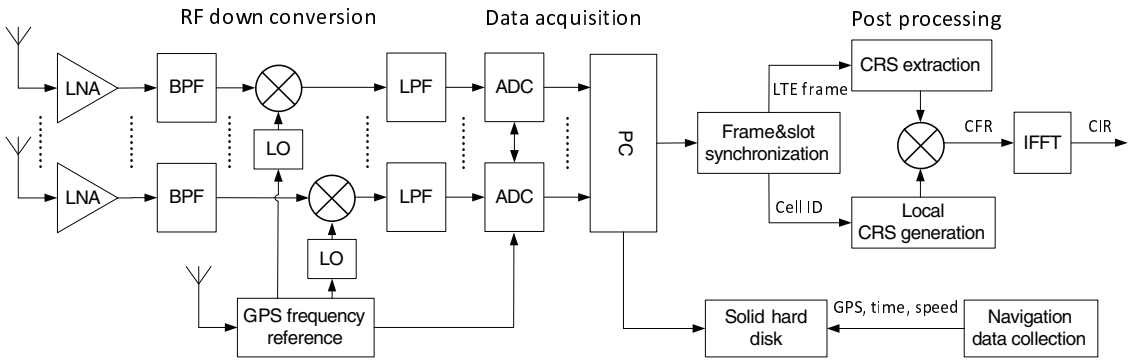

Fig. 2. Block diagram of LTE sounder.

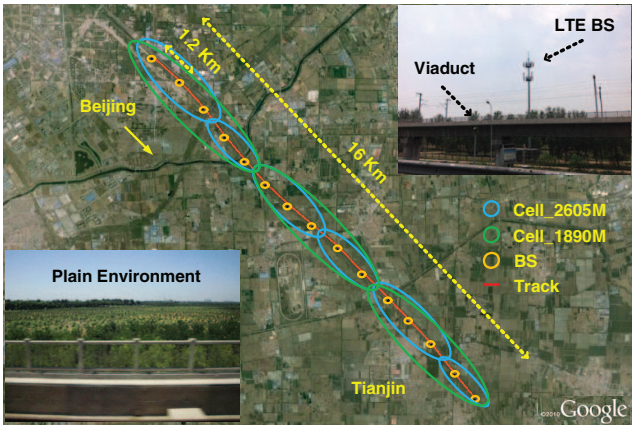

Fig. 3. LTE network structure and propagation environment on BT HSR.

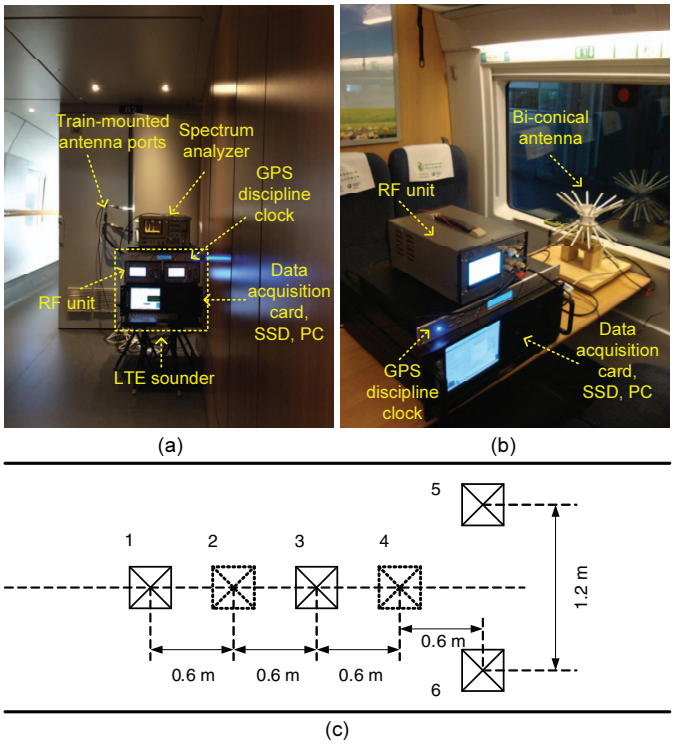

Fig. 4. Measurement equipment in the two scenarios. (a) RC case. (b) DC case. (c) Structure of train-mounted antennas. Antennas 1, 3, 5, 6 can be used for the wideband signal test, while antennas 2 and 4 can only be available for the specific GSM-R network.

1890 MHz network has 3 bigger cells with 5 BSs each. The BS is generally less than 20 m away from the rail which is built on viaduct. There are three typical BS heights, such as 10 m, 20 m and 35 m, which indicate the vertical distance between the BS antenna and the viaduct. Along the BT HSR, plain is the main propagation environment where there are usually a large range of open area, light forestation or a few buildings with an average height of less than 10 m.

Two possible HSR wireless coverage schemes [5], direct coverage (DC) and relay coverage (RC), are considered in the measurements. SISO channel measurements are carried out using the 2605 MHz network for the DC scenario, whereas 2×2 MIMO channel measurements are performed employing the 1890 MHz network for the RC scenario. Fig. 4 shows the measurement equipment in the two scenarios. The LTE sounder is built by a GPS discipline clock, two RF units, a data acquisition card, a SSD, and a PC. With regard to the DC measurement, a bi-conical antenna is utilized and placed inside the train carriage close to the window. As for the RC measurement, the LTE sounder adopts the professional train-mounted antennas whose structure is shown in Fig. 4(c). In the test, antennas 5 and 6 marked by red circles are chosen for the MIMO measurement, antenna 3 is connected to spectrum analyzer to monitor the signal state, and antenna 1 is used to receive the GPS signal. The detailed measurement parameters are listed in Table. 1.

B. Measurement Data Partitioning

Since the measurement data are collected in both the non-overlapping and overlapping areas of the network, they can be reasonably partitioned into two cases: single-link and multi-link measurement data. As shown in Fig. 5, we take an example of the power delay profile (PDP) result in one cell for the RC scenario to explain how to partition the measurement data. In Fig. 5(a), the time-variant PDP during the first 35 s period in the cell is plotted. Two obvious PDP transitions regarding BS1 and BS2 whose positions are identified by the white circles are highlighted. When the train enters into the

TABLE I
MEASUREMENT PARAMETERS

Measurement scenario	DC	RC
Measurement frequency	2605 MHz	1890 MHz
Measurement Bandwidth	18 MHz	18 MHz
CRS transmitted power	12.2 dBm	12.2 dBm
Transmit antenna type	$\pm 45^\circ$ cross-polarized	$\pm 45^\circ$ cross-polarized
Transmit antenna gain	18.6 dBi	17.4 dBi
Horizontal half-power beamwidth of transmit antenna	60°	67°
Vertical half-power beamwidth of transmit antenna	4.9°	6.6°
Electric tilted angle of transmit antenna	3°	3°
Receive antenna type	Bi-conical	HUBER+SUHNER
Receive antenna gain	0 dBi	8.5 dBi
Receive antenna number	1	2
Receive antenna spacing	-	1.2 m (7.6 wavelengths)
Train velocity	285 kmh	285 kmh

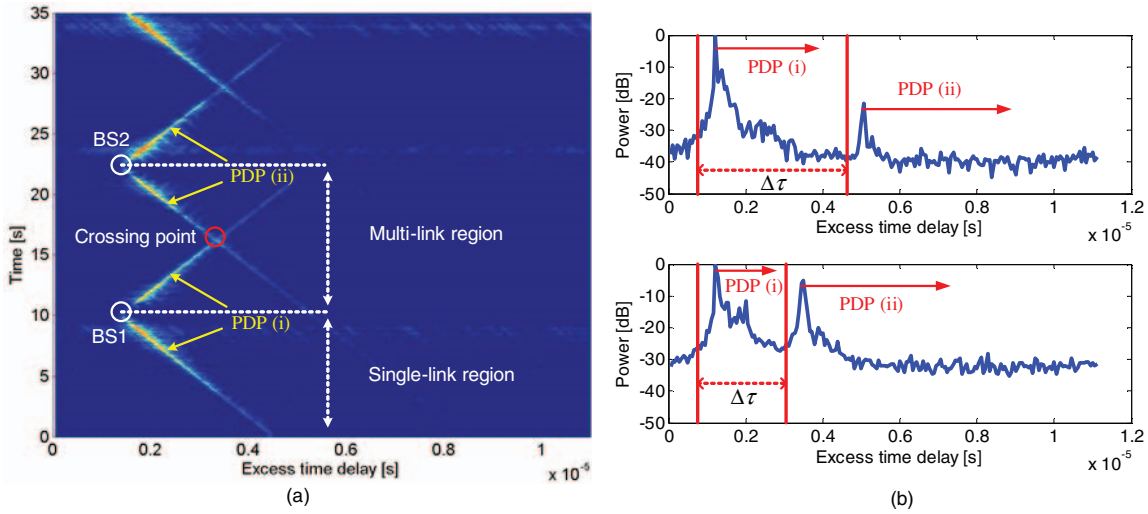

Fig. 5. Measured PDP in one cell for the RC scenario. (a) Time-variant PDP. (b) Two snapshots of the PDP in the multi-link region. The top one is captured when the train is close to BS1, whereas the bottom one is recorded when the train moves away from BS1.

non-overlapping area, we define a single-link region where the propagation link between BS1 and the train, indicated by PDP (i), almost occupies the whole time delay window. However, once the train moves into the overlapping area between BS1 and BS2, another propagation link between BS2 and the train, denoted by PDP (ii), appears in the time delay window as well. We regard this area as a multi-link region where the time delay window covers two links simultaneously. In the multi-link region, the time delay window can be divided into two parts: one is for PDP (i) and another is for PDP (ii), as shown in Fig. 5(b). As the train is moving away from BS1, the delay difference $\Delta\tau$ between PDP (i) and PDP (ii) is gradually shortening. If the train travels at the crossing point marked with a red circle in Fig. 5(a), the PDP (i) and PDP (ii) would be indistinguishable, e. g., $\Delta\tau = 0$. Since $\Delta\tau$ determines the time delay window of PDP (i), a threshold, $\Delta\tau = 1\mu s$, is set to enable the coverage of most multipath components.

In the single-link region we express the measured CIR matrix as H_{ij}^{S} and in the multi-link region we respectively extract the CIR matrices from BS1 and BS2 according to the above analysis, represented as $\mathrm{H}_{ij}^{M,1}$ and $\mathrm{H}_{ij}^{M,2}$. Note that i and j are the indices of the antenna elements at the BS and the LTE sounder. In addition, we choose 6 groups of DC measurement data and 3 groups of RS measurement data, each of which corresponds to one cell. Based on these data, in the following section we show the HSR channel characterization.

IV. LTE-Based HSR Channel Characterization

A. Path Loss

To extract the path loss (PL), the measured CIR should be averaged within a local area, where the condition of wide-sense stationary and uncorrelated scattering (WSSUS) is satisfied. The averaged length is commonly chosen to be 20 wavelengths in the mobile measurement [13]. Denoting the CRS transmitted power, transmit antenna gain, receive antenna gain as P_T, G_T, and G_R, the PL P_L can be calculated in dB as

$$P_L = P_T + G_T + G_R - 10\log_{10}\left(\sum_{\tau}\left|\tilde{h}_{11}^{S}(\tau)\right|^2\right), \quad (1)$$

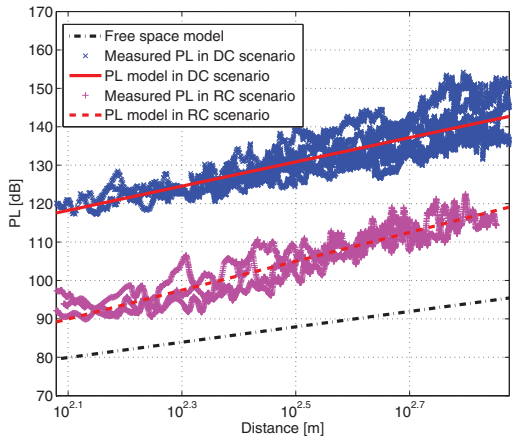

Fig. 6. PL for the DC and RC scenarios.

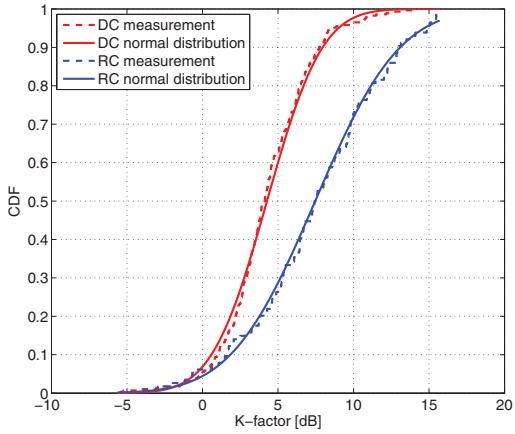

Fig. 7. CDF of K-factor for the DC and RC scenarios.

where τ is the delay index, $\tilde{h}_{11}^{S}(\tau)$ indicates the averaged CIR from the first transmit element to the first receive element in the single-link region.

The PL is conventionally modeled as a function of logarithmic distance. The estimated PL models in dB for the DC and RC scenarios are given as

$$P_L(d) = 51.9 + 31.6 \log 10(d) \tag{2}$$

and

$$P_L(d) = 11.2 + 37.6 \log 10(d), \tag{3}$$

where d is the distance between the BS and the train.

Fig. 6 illustrates the measured PL results and the PL models for the DC and MRC scenarios. It can be seen that the PL in the DC scenario is approximately 20-30 dB higher than that in the RC scenario. This value corresponds to the penetration loss from the train body. On the other hand, the resulting PL exponents for the DC and MRC cases are 3.16 and 3.76, respectively, which are all much higher than that of 2.0 in the free space model. For the DC it is understandable that the outdoor to indoor propagation condition intensifies the attenuation of signal power, however, for the MRC the main reason which has been explained in [3] [5] is that the train carriage roof would act as a ground plane and thus affect the antenna radiation pattern by causing a null in a certain incidence angle area of the radiation pattern.

B. Ricean K-factor

Ricean K-factor is a parameter indicating the temporal fading severity of the radio channel, which can be extracted by the CIR of removing the large-scale effect. The K-factor is estimated in the same set of 10 m windows using the classical moment based method in [14], as a function of distance.

Fig. 7 presents the cumulative distribution function (CDF) of the K-factors and the fitting of the CDF with a normal distribution for the DC and RC scenarios. A K-factor with a mean of 4.27 dB and a standard deviation of 2.87 dB is observed for the DC case, whereas they are 7.47 dB and 4.39 dB for the RC case. The strength of K-factor in the DC case is weaker than that in the BS-RS case because the receiver antenna inside the train carriage encounters more multipath echoes decreasing the K-factor. In addition, the K-factor result of RC matches the K-factor model with 7 dB mean value and 4 dB standard deviation for the RMa scenario in ITU-R M.2135 model [15].

C. RMS Delay Spread

The root mean square (RMS) delay spread (DS) is determined by the PDP at local area, which can be calculated as the standard deviation of the excess time delay weighted with the power [16].

Fig. 8 shows the CDF of the RMS DSs and the fitting of the CDF with a lognormal distribution for the DC and RC scenarios. It is obvious that the DC case has the higher RMS DS than the RC case since the indoor antenna receives more multipath waves. The fitting parameters $\mu(\log 10(\mathrm{s}))$ and $\sigma(\log 10(\mathrm{s}))$ of the RMS DS for the RC case are -7.68 and 0.57, whereas those for the DC case are -7.06 and 0.34. It can be found that the RC result is close to the ITU-R M.2135 model [15] in the RMa scenario with the mean value of -7.49 and the standard deviation of 0.55.

D. Spatial Correlation

To investigate the MIMO performance, we focus on the spatial correlation (SC) between the different antenna elements at both ends of the individual link, namely, single-link SC. Besides, we also consider the multi-link SC [17] which exists due to the environment similarity arising from common scatterers contributing to different links and can significantly affect the performance of coordinated multipoint transmission (CoMP) technology. Based on the measurement data in the single-link region, the single-link SC between two sub-channels, H_{11}^{S} and H_{22}^{S}, is derived. Similarly, according to the effective measurement data in the multi-link region, the multi-link SC between $\mathrm{H}_{11}^{M,1}$ and $\mathrm{H}_{11}^{M,2}$ is estimated. Fig. 9 illustrates the single-link SC result in the RC scenario and multi-link SC results in the DC and RC scenarios. It is observed that almost 65% of single-link SC values are less than 0.8. For the multi-link SC, the results are optimistic in both DC and RC scenarios

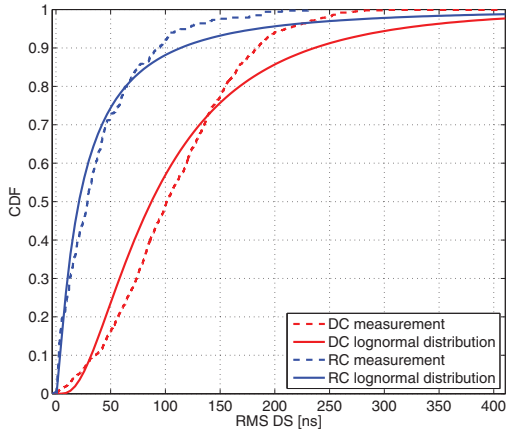

Fig. 8. CDF of RMS DS for the DC and RC scenarios.

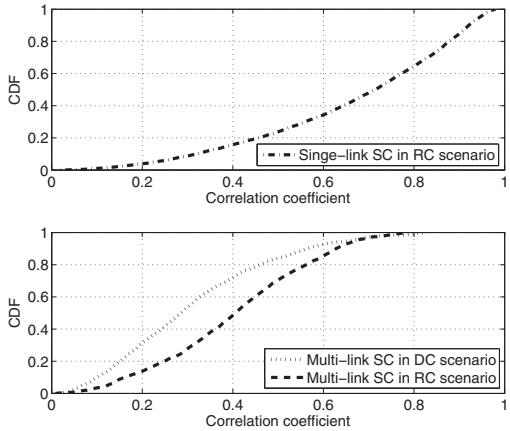

Fig. 9. CDF of SC for the DC and RC scenarios.

where the majority of the correlation coefficients are below 0.8. Moreover, since rich scatterers in the in-train environment lead to a low degree of environment similarity, the DC case has the lower multi-link SC than the RC case. From these results, we can infer that in the HSR scenario the MIMO performance could be improved by means of the cross-polarized antenna configuration at the BS side and the large antenna spacing at the train side. Moreover, CoMP technology could have a good performance in terms of micro-diversity due to the low multi-link SC.

V. Conclusion

In this paper, using a novel LTE-based HSR channel sounding system, field measurements taking DC and RC schemes into account were performed on Beijing to Tianjin HSR in China. Single-link and multi-link measurement data were collected and partitioned for the channel characterization. The measurement results proved the availability of the proposed system and provided some typical HSR channel features. First, both the DC and RC scenarios have much higher PL exponent than the free space propagation scenario. Besides, the RC case has the stronger K-factor but smaller RMS DS than the DC case. Moreover, the single-link SC of the HSR channel could be reduced in the case of the cross-polarized antenna configuration at the BS side and the large antenna spacing at the train side. Finally, the multi-link SC could be relatively low in the HSR scenario.

Acknowledgment

The research was supported in part by the NSFC projects under grant No. 61371070, No. 61471030, Beijing Natural Science Foundation (4142041, 4152043), and the open research fund of National Mobile Communications Research Laboratory, Southeast University (No.2014D05).

References

[1] B. Ai, X. Cheng, T. Kürner, Z. D. Zhong, K. Guan, R. S. He, L. Xiong, D. W. Matolak, D. G. Michelson, and C. B. Rodriguez, "Challenges toward wireless communications for high-speed railway," *IEEE Tran. Intell. Transp.*, vol. 15, no. 5, pp. 2143-2158, Oct. 2014.

[2] J. Y. Zhang, Z. H. Tan, Z. D. Zhong, and Y. Kong, "A multi-mode multi-band and multi-system-based access architecture for high-speed railways," In *Proc. IEEE 72nd Vehicular Technology Conf. (VTC Fall)*, Ottawa, Canada, Sept. 2010.

[3] P. Kyösti, "WINNER II channel models part II radio channel measurement and analysis results," 2007.

[4] R. Parviainen, P. Kyösti, and Y. Hsieh, "Results of high speed train channel measurements," European Cooperation in the Field of Scientific and Technical Research, Tech. Rep., 2008.

[5] L. Liu, C. Tao, J. Qiu, H. Chen, L. Yu, W. Dong, and Y. Yuan, "Position-based modeling for wireless channel on high-speed railway under a viaduct at 2.35 GHz," *IEEE J. Sel. Area. Comm.*, vol. 30, no. 4, pp. 834-845, May. 2012.

[6] L. Liu, C. Tao, T. Zhou, Y. P. Zhao, X. F. Yin, and H. J. Chen, "A highly efficient channel sounding method based on cellular communications for high-speed railway scenarios," *EURASIP J. Wireless. Commun.*, vol. 2012, 2012:307.

[7] R. S. He, Z. D. Zhong, B. Ai, and J. Ding, "An empirical path loss model and fading analysis for high-speed railway viaduct scenarios," *IEEE Antennas Wireless Propag. Lett.*, vol. 10, pp. 808-812, Aug. 2011.

[8] J. H. Qiu, C. Tao, L. Liu, and Z. H. Tan, "Broadband channel measurement for the high-speed railway based on WCDMA," In *Proc. IEEE 75th Vehicular Technology Conf. (VTC Spring)*, Yokohama, Japan, May 2012.

[9] [Online]. Available: http://www.huawei.com/za/static/HW-371906.pdf

[10] T. Zhou, C. Tao, L. Liu, and Z. H. Tan, "A study on a LTE-based channel sounding scheme for high-speed railway scenarios," In *Proc. IEEE 78th Vehicular Technology Conf. (VTC Fall)*, Las Vegas, USA, Sept. 2013.

[11] S. Salous, Radio Propagation Measurement and Channel Modelling, John Wiley and Sons Ltd., Wiley, 2013.

[12] [Online]. Available: http://www.channelsounder.de/csprinciple_site2.html

[13] X. Zhao, J. Kivinen, P. Vainikainen, and K. Skog, "Propagation characteristics for wideband outdoor mobile communications at 5.3 GHz," *IEEE J. Sel. Areas Commun.*, vol. 20, no. 3, pp. 507-514, Apr. 2002.

[14] L. Greenstein, D. Michelson and V. Erceg, "Moment-method estimation of the Ricean K-factor," *IEEE Comm. Lett.*, vol. 3, no. 6, pp. 175-176, 1999.

[15] ITU-R M.2135, Guidelines for evaluation of radio interface technologies for IMT-Advanced, 2009.

[16] J. H. Zhang, D. Dong, Y. P. Liang, X. Nie, X. Y. Gao, Y. Zhang, C. Huang, and G. Y. Liu, "Propagation characteristics of wideband MIMO channel in urban micro- and macrocells," in *Proc. IEEE International Symposium on Personal, Indoor and Mobile Radio Communications (PIMRC)*, Cannes, France, Sept. 2008.

[17] X. Cheng, C.-X. Wang, H. Wang, X. Gao, X.-H. You, D. Yuan, B. Ai, Q. Huo, L. Song, and B. Jiao, "Cooperative MIMO channel modeling and multi-link spatial correlation properties," *IEEE J. Sel. Areas Commun.*, vol. 30, no. 2, pp. 388-396, Feb. 2012.